2025 IEEE/SICE International Symposium on System Integration (SII)
January 21-24, 2025, Munich, Germany

Enhancing Teleoperator Awareness of Gripper-Object Interaction by Modulating Control Button Stiffness

Noel Alejandro Avila Campos[1], Masashi Konyo[1], Ranulfo Bezerra [1], Shotaro Kojima[1], Satoshi Tadokoro[1]

Abstract— **This study addresses the challenge of limited dexterity in teleoperation tasks caused by the absence of sensory feedback and visual occlusions. Our approach anticipates interactions by virtually enlarging the robot's gripper and calculating the overlapping volume with nearby objects. To intuitively convey this information to the operator in real time, we employ haptic feedback by adjusting the stiffness of the controller's buttons based on the proximity of the detected objects. The system has been tested in a simulation environment with the aim of achieving a good position to grasp a target. In situations where the target was not fully grasped, operators using haptic feedback reached the "Best" position 28% faster than those without it, indicating enhanced situational awareness and control. The percentage of the target inside the gripper was notably higher, and centering and alignment errors were minimized, suggesting more precise grasping with less damage to the robot or the object. Although the collision frequency remained similar, the severity of collisions—both maximum and average—was reduced when haptic feedback was employed. In situations where the target was fully grasped, there are minor differences when performing with or without haptic feedback. These findings suggest that haptic feedback improves the user's awareness of the robot's interactions with its environment and enhance the operator's ability to make informed decisions.**

I. INTRODUCTION

Teleoperation enables remote control of robots, crucial for tasks in hazardous or complex environments like nuclear energy, underwater operations, tele-surgery. and rescue and safety missions [1], [2]. Efficient execution of these tasks requires a degree of dexterity, which varies depending on the specific activity.

Dexterity has been a key topic in robotics [3], and in this paper, we define it similarly to manual dexterity: the ability to manipulate objects using the hands and fingers to perform movements with precision and in a timely manner according to the task requirements [4]. These movements must be highly controlled and responsive to the surrounding environment.

Low dexterity in robot movements can result in direct damage to the robotic system, its environment, or the objects with which it interacts. If the robot lacks a proper proprioceptive system, undetected collisions not only cause damage but also increase the discrepancy between the estimated and actual positions.

One of the main reasons for reduced dexterity in teleoperation is that the operator cannot feel what the robot is experiencing. Since the operator is not physically present in the robot's environment, they rely solely on the information provided by the robot. When interacting with objects, the robot's arm often obstructs the operator's view, a phenomenon known as occlusion. Moreover, visual information alone is often insufficient to perceive the depth of objects. Solutions like adding extra cameras increase the complexity of stimuli received by the operator, thereby raising cognitive load and worsening performance [5].

The primary issue in teleoperation tasks is the reduced dexterity of the robot, which leads to damage to both the robotic system and its environment. This is due to the operator's lack of sensory feedback, which hinders their perception of the robot's interactions. Furthermore, visual occlusion, where the robot's arm blocks the operator's view, complicates the task. Attempts to compensate with adding more cameras tend to increase the operator's cognitive load. As a result, both the precision and efficiency of operations are reduced, even though these are critical due to the importance and urgency of the tasks.

To address collision avoidance, various approaches have been proposed. For example, artificial force fields have been used to guide unmanned aerial vehicles (UAVs) or vertical take off and landing capabilities (VTOL) and prevent collisions [6], [7]. Similarly, haptic guidance systems, based on the surface's normal force, have been developed to push users away from obstacles and toward safe paths [8]. These methods are further enhanced with dynamic artificial potential fields that predict user intentions and automatically adjust trajectories to avoid obstacles [9].

Other research focuses on haptic and sensory feedback. A haptic device has been introduced to provide both contact location and force feedback to improve natural interaction [10]. Studies also explore the impact of varying levels of haptic force on teleoperation performance [11], while other work combines haptic cues with augmented reality (AR) visual feedback to enhance control and reduce cognitive load in telemanipulation tasks [12].

This study proposes a method to enhance the user's awareness of the robot's interactions with its environment, with a particular focus on the gripper to avoid collisions and improve object handling. This leads to an overall improvement in the robot's dexterity. The method integrates

*This research was performed by the commissioned research fund provided by F-REI (#JPFR23010101)

[1]Graduate School of Information Sciences, Tohoku University, Sendai, Japan. avila.noel@rm.is.tohoku.ac.jp, konyo@rm.is.tohoku.ac.jp, bezerra.ranulfo@rm.is.tohoku.ac.jp, kojima@rm.is.tohoku.ac.jp, tadokoro@rm.is.tohoku.ac.jp

haptic feedback that reflects the relationship between the robot's end-effector and nearby objects. By incorporating this feedback, the operator is expected to gain a more intuitive understanding of the environment, enhancing their control over the robot's actions.

The proposed technology predicts interactions by virtually enlarging the robot's gripper and calculating its volume overlap with surrounding objects. The teleoperator's input method is used to provide haptic feedback, delivering this information to the user intuitively and in real time. The feedback is generated by adjusting the stiffness of the controller's buttons of the direction of nearby objects based on the calculated volume intersection. The system is designed to have low complexity, using simplified approaches that can operate in parallel to real executions.

II. METHODOLOGY

To enhance the user's awareness of the environment in which the teleoperated robot performs, it is essential to gather detailed information about the surroundings and nearby objects. We rely on a simulation of the robot and its environment to collect data, which can be achieved using depth cameras, radars, and segmentation models. The recognized objects should be represented by simple geometric shapes such as spheres, hexahedrons, parallelepipeds, or cubes. In the other hand, the position of the end-effector is estimated based on a model of the robot based on its current configuration. Both the estimated position of the objects and that of the end-effector inherently carry errors. Subsequently, the neccesity of a method to effectively convey the collected information to the user arose. This study assumes that the position and shape of objects near the robot have been previously collected, focusing on the processing and transmission of this information while minimizing the impact of modeling errors.

A. SIMULATION

The simulation mirrors the teleoperated environment using virtual models of the robot and objects, detected via depth cameras and segmentation models. The gripper's ends are enlarged in the virtual space to detect its colision before it happens in reality and provide lateral directional haptic feedback to the operator. When an object is near one side of the gripper, only the corresponding control button stiffens, signaling lateral proximity. If the object is centrally positioned and close to both ends, both buttons stiffen simultaneously, effectively conveying the object's position without compromising feedback precision.

Given the error in the estimation of the position of a camera by the device's specification:

$$\mathrm{Cam}_{\mathrm{Err}} = x_{\mathrm{real}} - \hat{x}_{\mathrm{est}} \tag{1}$$

Assuming it behaves as a normal distribution:

$$\mathrm{Cam}_{\mathrm{Err}} \sim \mathcal{N}(\mu_c, \sigma_c^2) = \frac{1}{\sigma_c\sqrt{2\pi}} \exp\left(-\frac{(x-\mu_c)^2}{2\sigma_c^2}\right) \tag{2}$$

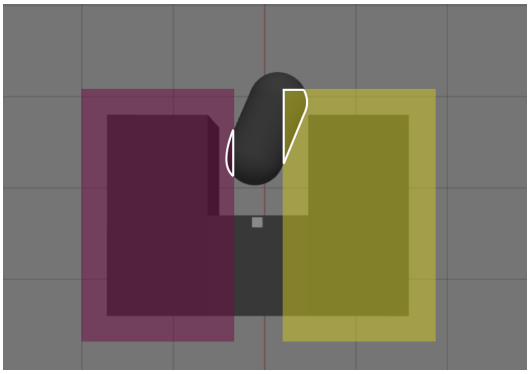

Fig. 1: Volume Enlargement

B. End-Effector Position estimation

As the state of the end-effector is essential, a precise estimation of the current position and orientation of the end-effector can be based on the joint angle information. Additionally, the distribution of the position error of the end-effector can be estimated through error propagation.
Given: θ_i = angle of the joint i-th.

The difference between the actual and estimated angles can be quantified by the error specified in the encoder's characteristics.

$$\Delta\theta_i = \theta_i - \hat{\theta}_i \tag{3}$$

Given: $T_i = \text{Transformation matrix of joint } i$

The direct kinematics as a series of transformation matrices:

$$T_{\mathrm{total}} = T_1 T_2 \cdots T_{n-1} T_n \tag{4}$$

Where: The propagation of errors is defined by [13]:

$$\sigma_p = \sqrt{\sum_{i=1}^{n} \left(\frac{\partial p}{\partial \theta_i}\Delta\theta_i\right)^2} \tag{5}$$

Where: p: The standard deviation of the error in the end-effector's position estimation. $\frac{\partial p}{\partial \theta_i}$: Derivative of position with respect to i-th angle.

The error of the end effector position estimation by direct kinematic would correspond to:

$$\Delta T_{ee,k} \equiv T_{ee} - \hat{T}_{ee,k} \tag{6}$$

Assuming it as a normal distribution, its model is:

$$\Delta T_{ee,k} \sim \mathcal{N}(\mu_{ee}, \sigma_p^2) \tag{7}$$

C. Delay displacement consideration

We should also consider the unavoidable delay in teleoperation to correctly calculate the difference in position between the robot and its virtual counterpart.

$$\Delta T_{ee,d} \equiv \frac{dx}{dt} \cdot t_d \tag{8}$$

D. Enlargement Distance

Then, we enlarge the virtual model of the detected objects and environment. The enlargement's distance should be big enough to overcome the estimated position error, the discrepancy of the virtual object with its physical counterpart, and the delay in communication to prevent any possible collision. Nevertheless, the distance should be small so as not to slow down the whole performance of the robot more than convenient. Another parameter to consider is the distance between both sides of the robot's gripper; otherwise, the enlarged volume could cause interference between them. As the contact depends on the relation of both objects, all considered errors should be considered. We combine normal distributions for the camera and end effector position estimation, equations (2), (7), and (8). We applied the following mathematical approach to set the distance for enlargement. Based on the safety parameter P, which represents the probability requirement for preventing undesired contact, the enlargement distance is defined by:

$$D_{\text{incr}}(P) \approx \Delta T_{ee,d} + (\Delta T_{ee,k})^{-1} + (\text{Cam}_{\text{Err}})^{-1} \quad (9)$$

$$D_{\text{incr}}(P) \approx \Delta T_{ee,d} + \Phi^{-1}(P, \mu_{ee} + \mu_c, \Delta p^2 + \sigma_c^2) \quad (10)$$

Where:

- P: Probability for preventing collision ($P \in [0, 1]$).
- Φ: Cumulative distribution function (CDF) until P [14].

$$\Phi(P, \mu, \sigma^2) = \int_{-\infty}^{P} \frac{1}{\sigma\sqrt{2\pi}} \exp\left(-\frac{(t-\mu)^2}{2\sigma^2}\right) dt$$

It is worth mentioning that the enlargement distance is calculated only once based on the robot to be implemented based on the sensors' information.

E. Volume intersection calculation

As the objects in the simulation can be modeled as basic shapes, the volume intersection in three dimensions can be calculated by applying analytical methods. Given the case that the objects are modeled as spheres and hexahedra on the simulation, the intersection between those shapes is defined as follows.

$$V_{\text{Overlap}} = \int_{\text{Hex}} H(R^2 - ((x-x_0)^2 + (y-y_0)^2 + (z-z_0)^2))dx\,dy\,dz \quad (11)$$

Where:

- V_{OL} = The volume overlap
- $H(x)$ = The Heaviside function.
  - $H(x) = 1 \quad \text{for } x \geq 0$
  - $H(x) = 0 \quad \text{for } x < 0$
- R = Sphere's radius
- (x_0, y_0, z_0) = Coordinates of the sphere's center
- Hex = Hexahedron's coordinates

As the objects are simplified as spheres and boxes, we can lower the algorithm's complexity by applying the following approximation [15].

$$V_{\text{overlap}} = V_s - \sum_{\text{faces}} V_c + \sum_{\text{edges}} V_w - \sum_{\text{vertices}} V_{co} \quad (12)$$

Where:

- V_s = Volume of the sphere
- V_c = Volume of the cap
- V_w = Volume of the wedge
- V_{co} = Volume of the cone

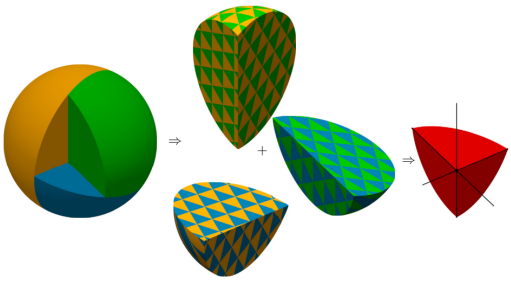

Fig. 2: Sphere's volume overlap calculation [15]

F. Haptic Feedback

To intuitively convey information to the user, we use a haptic feedback mechanism. It adjusts the stiffness of the control buttons used to teleoperate the robot. As the virtual volume intersection with an object increases, the designated button becomes proportionally stiffer. For example, the closer the object, the larger the intersection, and the stiffer the button turns. It is crucial to consider the correlation between the robot's movements and the buttons that control those movements. Haptic feedback should be applied to the button that causes the increase in intersection volume. This design encourages moving the end-effector away from other objects or adjusting its position relative to the target object. As a result, it helps prevent collisions and improves the parallelism and centering of the object to be grasped.

III. Experiment

A. Setup

1) Simulation: The experiment was conducted using ROS (Robot Operating System) in conjunction with Gazebo. To evaluate collisions, the ODE (Open Dynamics Engine) physics engine was employed within Gazebo to calculate the interaction between objects and retrieve information of the collisions inside the simulation.

2) Enlargement distance calculation: As shown in Equation (10), the following values allow for the calculation of the enlargement distance $D_{\text{incr}}(P)$:

$\Delta T_{ee,d}$, the term related to the robot's movement speed and delay time, is calculated by (8). In this case, the robot's speed is $\frac{dx}{dt} = 0.9\,\text{m/s}$, but only 30% of that speed is utilized during operations. Furthermore, a delay time of $t_d = \frac{1}{30}$ seconds is applied, leading to the result:

$$\Delta T_{ee,d} = \frac{dx}{dt} \cdot t_d = 0.9 \times 0.3\,\text{m/s} \times \frac{1}{30}\,\text{s} = 0.009\,\text{m} \quad (13)$$

$\Phi^{-1}(P, \mu, \sigma^2)$ is the inverse function of the normal CDF, in which $P = 0.9$, selected to represent a high probability threshold, ensuring that the enlargement distance is calculated with sufficient conservatism to account for potential uncertainties. Alternatively, μ_c is the camera error mean, it has a value of 0 for this case. The variance is calculated given the depth sensor accuracy [16], less than 2% at a distance of 2 meters. Calculating $\Delta p^2 \approx (0.02 \times 2)^2 = 0.0016$. Then $\sigma = \sqrt{0.0016} = 0.04$. Using standard normal CDF tables, for $P = 0.9$, $\mu = 0$, and $\sigma = 0.04$, we obtain:

$$\Phi^{-1}(P, \mu, \sigma^2) = \Phi^{-1}(0.9, 0, 0.04^2) \approx 0.011 \quad (14)$$

Finally, the resultant value of $D_{\text{incr}}(P)$ is computed as:

$$D_{\text{incr}}(P) \approx \Delta T_{ee,d} + \Phi^{-1}(P, \mu_{ee} + \mu_c, \Delta p^2 + \sigma_c^2) = \\ = 0.009 + 0.011 = 0.02\,\text{m} = 20\,\text{mm} \quad (15)$$

Therefore, the enlargement of volume of both models is $D_{\text{incr}}(P) = 20\,\text{mm}$.

3) Models (Onix, Target): The real Onix robot is described in [17]. For the virtual counterpart, a graphical representation of Onix was used in the simulation. For the gement and interception calculation, the gripper was modeled using two parallelepiped, as depicted in Fig. 3. For the Grip width not to affect on the collision performance of the subjects in the experiment, it was fixed to 100 mm for all the execution of the task.

The target object intended for grasping is a capsule-shaped item composed of two spheres with a 30 mm radius and a cylinder 60 mm in height. It's volume is virtually enlarged by 20 mm in all directions as shown in Fig 4. For the performance of users not to diverge in an unpredictable way based on their interactions within the objects, it's position is fix on the simulation.

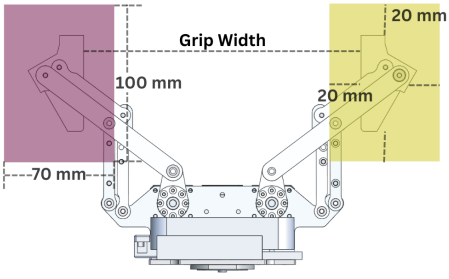

Fig. 3: Onix gripper with virtual volume intersection [17]

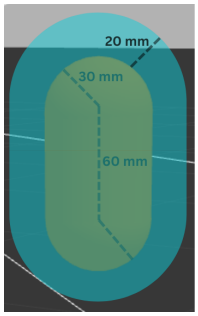

Fig. 4: Target Object

4) Cameras and Perspectives: Two screens were used during the experiment:

- **Left Screen:** Displayed an isometric view of the target object and the Onix robot within the Gazebo environment.
- **Right Screen:** Showed five perspectives from cameras mounted on the robot, replicating the real-life setup of the Onix robot. The left panel provided depth information from the gripper's camera. The upper image displayed data from the RealSense Color camera, capturing the color and shape of objects, while the lower image showed data from the RealSense Depth camera, indicating object distances using grayscale.

The upper panel displayed perspectives from three fisheye cameras: the ElbowCamera0 and ElbowCamera1 (showing front and rear views from the elbow of the Onix robot's manipulator) and the front chassis camera, as seen in Fig. 5.

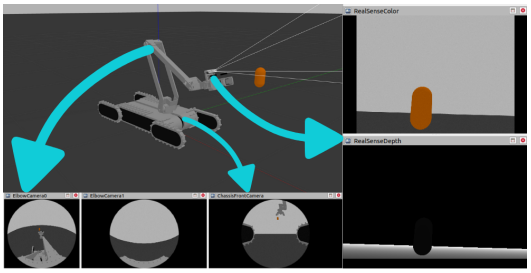

Fig. 5: Visual Feedback in the simulation

B. Hardware - DualSense

The PlayStation 5 DualSense controller, featuring adaptive triggers on "R2" and "L2," was utilized for this study. These triggers incorporate an internal mechanical system that adjusts the stiffness of the buttons, enabling haptic feedback proportional to the volume intersection near the robot's end effector (Fig. 6). The feedback buttons were also used to control the yaw rotation of the robot's end effector, providing precise maneuverability. The joystick-type design of the DualSense makes it particularly effective for controlling movements in multiple dimensions due to its intuitive and ergonomic configuration. Additionally, its availability, affordability, and ease of replacement enhance its practicality for research and operational use, offering a reliable and accessible tool for applications requiring precise control.

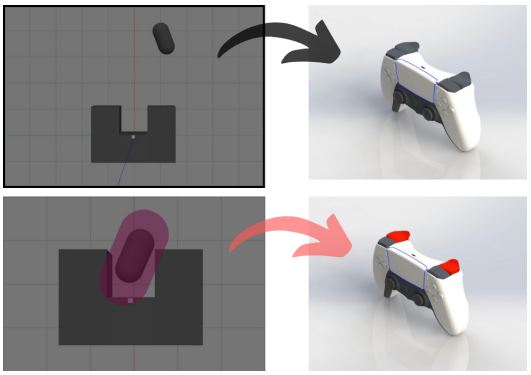

Fig. 6: Stiffness buttons in DualSense Controller

C. Stage 0 - Training

1) Control Movements: At the beginning of each session, participants could test the controls to familiarize themselves

with the robot's movements. The control allowed manipulation across three axes of rotation and orientation of the end-effector. A chart was provided for reference to help participants master the control of the robot.

2) Feedback Axis Selection: The yaw axis was chosen for haptic feedback because it allows the robot to rotate without incurring collisions in previously safe positions. Additionally, it provides clear feedback on the object's position relative to the end effector, crucial for aligning the gripper with the target object.

For both haptic feedback and non-haptic feedback trials, participants were instructed to keep the R2 and L2 triggers pressed. As the stiffness of these triggers changed, users could feel the adjustment. To rotate left, the participant would partially release the left trigger in a controlled manner, as the trigger is analog and does not require full release, the haptic stimulus remains perceivable. If both triggers were pressed with the same force, the end-effector would not rotate. This approach is similar to a dead man's switch, ensuring the operator maintains active control of the robot.

Before haptic feedback trials, participants received training on using the haptic stimuli and understanding its calculation. This training was provided either before the first or third stage, depending on the experiment setup.

D. Task

1) Objective: Participants positioned the gripper to grasp the target object quickly, avoiding contact and ensuring proper centering and alignment. The supervisor reset the object between tasks upon completion.

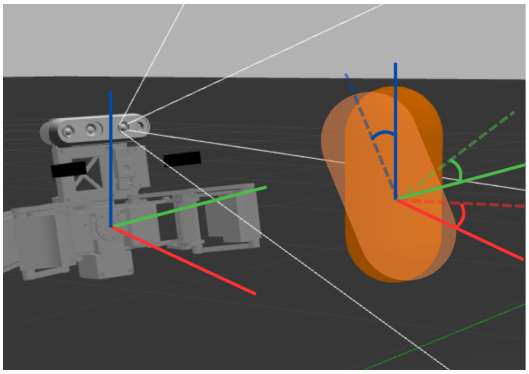

Fig. 7: Robot and Target object Angle comparison

2) Spawn Area: At the start of each task, the object was placed in front of the robot, within the range [0.9-1.1, 0.34-0.36, 0.35-0.70] (check Fig. 8) with a roll rotation of up to 7 degrees. This area was visible from the robot's front camera, and the object's distinctive orange color made it stand out against the background.

3) Strategy and Trajectory: Participants were instructed to return the end-effector to the front of the robot when seeking and aligning with the object to avoid getting stuck or blocked. The object had to be grasped frontally, not from above or below.

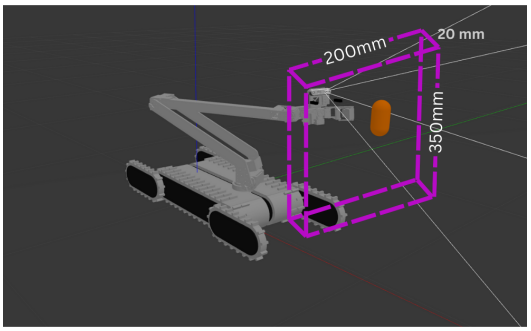

Fig. 8: Spawn Area

4) Stages and Repetitions: The experiment consisted of four stages, designed to evaluate the influence of haptic feedback on task performance. Each stage involved repetitive tasks where participants positioned the robot's end effector in preparation for grasping a virtual object, aiming to complete the task quickly, avoid collisions, and to position the gripper as perpendicularly and centrally as possible to the object.

Participants were randomly assigned to one of two groups to control for chronological performance influence:

Group 1: Haptic Feedback First: Trained with haptic feedback in Stage 1, followed by experimental tasks with haptic feedback in Stage 2. Then, they trained without haptic feedback in Stage 3 and completed experimental tasks without haptic feedback in Stage 4. Group 2: Haptic Feedback Second: Followed the reverse order, starting without haptic feedback in Stages 1 and 2, and using haptic feedback in Stages 3 and 4. Each training stage required at least 8 tasks, with 5 correct executions (e.g., proper button-movement correlation) to proceed. Experimental stages involved 5 consecutive tasks under the assigned conditions, without supervisor intervention. In total, each participant completed 26 tasks: 8 for training, 10 experimental, and 8 intermediate tasks.

IV. Data Analysis

A. Collected Data

For each task execution, the timestamp, intersection volume between the object and the parallelepipeds modeling the end-effector, intersection volume between the object and the interior area of the gripper, the distance between the two objects, and the roll, pitch, and yaw of the gripper at each simulation moment were recorded.

Each collision was recorded with object names, coordinates, normals, depth, and timestamp using the ODE physics model in Gazebo.

B. Error Indicators

The error was calculated by summing two measures: how aligned and centered the object was with the gripper. The alignment was quantified by calculating the angle between the gripper's y-axis and the object's z-axis. The value was normalized by dividing by $\pi/2$. The centering was quantified

using the asymmetry coefficient of the intersection volume between the object and the right and left parallelepipeds of the end-effector, according to the relation $(V_L - V_R)/(V_L + V_R)$. This value is naturally normalized. If both values are zero, the error is defined as 1, representing the maximum error.

C. Event Identification for Future Analysis

Events were identified to analyze the object approach and key points of interest in this study, such as the number and magnitude of collisions, and how centered and aligned the object was relative to the gripper. The time between these events was calculated, along with which collisions corresponded to each stage.

- **"Best" Event:** Defined by the object having at least a 0.03m radius sphere (0.000131m³) inside the gripper's grasp area and the smallest error.
- **"Find" Event:** Characterized by the user knowing the precise location of the object and moving towards it frontally. It precedes the "best" event and occurs when the distance is at least 0.3m.
- **"Enter" Event:** Occurs between "find" and "best" when at least one 0.03m radius sphere (0.000131m³) is within the gripper's grasp area.
- **"Last" Event:** The final data point of the trial when the user decides to stop, indicating task completion.

D. Summary of Analyzed Information

For each trial, the total time, partial times between start, find, enter, best, and last events were quantified. For these moments, the object's volume within the gripper, the distance between the objects, and the error in centering, alignment, and total error were recorded. For collision analysis, the quantity, average duration, maximum depth, and weighted average depth concerning duration were calculated.

V. Results

This section presents the results of a comparative analysis of key variables under different experimental conditions on the Table I. The variables include total time, volume inside the gripper, normalized alignment, normalized angle difference, collision frequency, maximum collision depth, and collision integral by time. These variables were analyzed by comparing three distinct contexts: first, comparing the presence or absence of haptic feedback on the execution of the task, to assess the impact of this technology on performance; second, comparing the order in which the tasks was performed, distinguishing between actions executed on the first and second condition and to indirectly evaluate the impact of the learning curve; and third, evaluating whether the target was fully inside the gripper, providing insights into how precision in manipulation affects outcomes. Each table provides the mean values and standard deviations of the variables under study, as well as Cohen's d statistic to compare the magnitude of the observed differences.

In addition to Table I, a multivariable study was conducted between the "Find" and "Best" moments, considering only cases where the target did not fully enter the gripper.

A graphical comparison was made between cases with and without haptic feedback. A boxplot was chosen to visually identify the median and to enable the comparison of corresponding cases (e.g., comparing the worst with the worst, the second worst with the second worst, etc.) between the two groups. The results of this comparison are presented in Fig. 9:

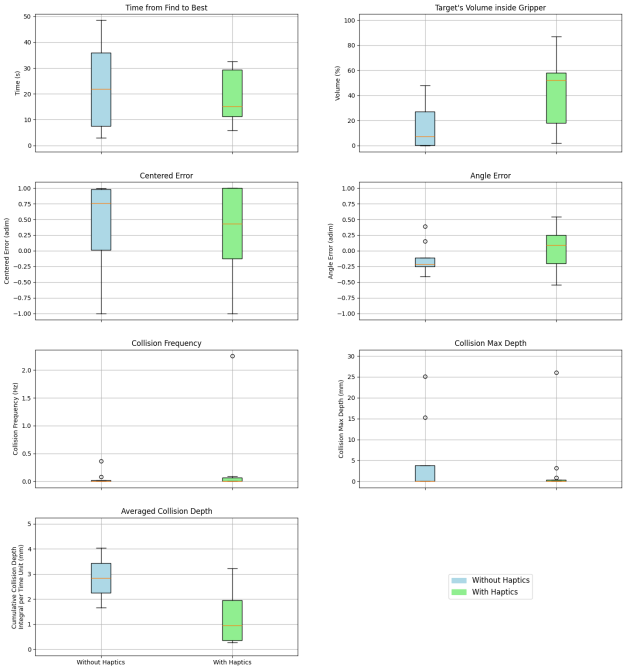

Fig. 9: Boxplots comparing the impact of haptic feedback on multiple metrics in situations where the target did not fully enter the grasp area of the gripper

VI. Discussion

In Figure 9, the benefits of using haptic feedback to convey the environment around the end effector to the teleoperator can be observed. With haptic feedback, the time between finding the object and reaching the "Best" position is notably shorter. The percentage of the target inside the gripper is also higher with haptic feedback. Centering and alignment errors are closer to zero. The collision frequency remains at similar values, except for some outliers. The severity of collisions, both maximum and average, is lower with haptic feedback.

To analyze the area of interest of this document, we should focus especially on the columns "To Enter" and "To Best" in Table 1. The "Total" section provides an overview of performance throughout the entire task. In "To Find" and "To Last," there is too much variation, and they do not represent the crucial moment of the desired interaction, which is inserting the target into the gripper and adjusting it. It is observed that the time difference between with and without haptic feedback is at "Best," with a reduction of 28%. Also, as expected, execution in the second condition is 20% faster, which demonstrates the learning process the subjects were undergoing.

TABLE I: Data Comparative Analysis

Description	Total	To Find	To Enter	To Best	To Last
Time (s)					
No Haptics	74.04 ± 62.22	49.35 ± 55.83	18.30 ± 13.46	1.68 ± 2.58	4.72 ± 9.02
Haptics	73.28 ± 54.10	44.11 ± 43.63	17.82 ± 13.08	1.21 ± 1.59	10.14 ± 35.38
Cohen's d	-0.0131	-0.1260	-0.0422	-0.2220	0.3650
First	86.50 ± 59.62	58.13 ± 53.07	20.83 ± 14.86	1.57 ± 2.57	5.97 ± 11.80
Subsequent	60.82 ± 53.88	35.33 ± 44.16	15.29 ± 10.75	1.31 ± 1.63	8.89 ± 34.71
Cohen's d	0.4520	0.4671	0.4275	0.4450	0.0905
Insufficiently grasped	88.78 ± 78.78	53.74 ± 65.16	20.64 ± 13.16	0 ± 0	14.40 ± 43.09
Target grasped	66.10 ± 43.07	43.22 ± 40.48	16.77 ± 13.13	2.17 ± 2.30	3.94 ± 7.81
Cohen's d	-0.3572	-0.1938	-0.2942	-0.1279	1.3297
Volume Inside Gripper (mm^3)					
No Haptics	2.26 ± 1.81	0 ± 0	0.80 ± 0.41	1.69 ± 1.60	2.26 ± 1.81
Haptics	1.69 ± 1.60	0 ± 0	0.78 ± 0.41	1.42 ± 1.17	1.69 ± 1.60
Cohen's d	-0.3331		-0.1820	-0.3265	-0.3331
First	1.94 ± 1.57	0 ± 0	0.82 ± 0.35	1.79 ± 1.45	1.94 ± 1.57
Subsequent	2.00 ± 1.87	0 ± 0	0.76 ± 0.40	1.88 ± 1.63	2.00 ± 1.87
Cohen's d	-0.0605		-0.0557	-0.0557	-0.0605
Insufficiently grasped	0.32 ± 0.27	0 ± 0	0.32 ± 0.28	0 ± 0	0.32 ± 0.27
Target grasped	2.86 ± 1.43	0 ± 0	1.03 ± 0.79	2.45 ± 2.16	2.86 ± 1.43
Cohen's d	2.5891		2.3546	1.3297	2.5891
Alignment (Norm.)					
No Haptics	0.2699 ± 0.6717	1.0 ± 0.0	0.2477 ± 0.6866	0.2462 ± 0.6099	0.2699 ± 0.6717
Haptics	0.3532 ± 0.6150	1.0 ± 0.0	0.3303 ± 0.6258	0.2554 ± 0.5302	0.3532 ± 0.6150
Cohen's d	-0.1292		-0.1258	-0.0162	-0.1292
First	0.4808 ± 0.5414	1.0 ± 0.0	0.4946 ± 0.5731	0.4139 ± 0.5158	0.4808 ± 0.5414
Subsequent	0.1423 ± 0.6933	1.0 ± 0.0	0.1294 ± 0.6857	0.1336 ± 0.5924	0.1423 ± 0.6933
Cohen's d	0.5442		0.5780	0.5046	0.5442
Insufficiently grasped	0.278 ± 0.792	1.0 ± 0.0	0.330 ± 0.737	0.330 ± 0.737	0.278 ± 0.792
Target grasped	0.327 ± 0.567	1.0 ± 0.0	0.270 ± 0.618	0.214 ± 0.474	0.327 ± 0.567
Cohen's d	0.0708		-0.0875	-0.1862	0.0708
Angle Difference (Norm.)					
No Haptics	0.0058 ± 0.3332	-0.0138 ± 0.3206	0.0048 ± 0.3155	-0.0003 ± 0.3054	0.0058 ± 0.3332
Haptics	0.0039 ± 0.3756	0.0260 ± 0.3735	-0.0076 ± 0.3553	-0.0082 ± 0.3602	0.0039 ± 0.3756
Cohen's d	0.0052	-0.1143	0.0369	0.0239	0.0052
First	0.1142 ± 0.3393	0.0919 ± 0.3062	0.1004 ± 0.3161	0.1001 ± 0.3223	0.1142 ± 0.3393
Subsequent	-0.1045 ± 0.3349	-0.0681 ± 0.3706	-0.0923 ± 0.3293	-0.0977 ± 0.3174	-0.1045 ± 0.3349
Cohen's d	0.4520	0.2439	0.1535	0.0905	0.4520
Insufficiently grasped	-0.0317 ± 0.302	0.0021 ± 0.362	-0.0381 ± 0.292	-0.0381 ± 0.292	-0.0317 ± 0.302
Target grasped	0.0218 ± 0.375	0.0080 ± 0.342	0.0156 ± 0.353	0.0114 ± 0.350	0.0218 ± 0.375
Cohen's d	0.1571	0.0169	0.1659	0.1538	0.1571
Collision Frequency (Hz)					
No Haptics	0.0643 ± 0.1189	0.0031 ± 0.0133	0.0151 ± 0.0387	0.0234 ± 0.0479	0.0407 ± 0.0518
Haptics	0.0708 ± 0.1012	0.0004 ± 0.0024	0.0188 ± 0.0513	0.0300 ± 0.0691	0.0519 ± 0.0583
Cohen's d	-0.0588	0.2752	-0.0809	-0.1110	-0.1507
First	0.0750 ± 0.0749	0 ± 0	0.0140 ± 0.0469	0.0419 ± 0.0562	0.0607 ± 0.0748
Subsequent	0.0601 ± 0.0601	0.0026 ± 0.0115	0.0248 ± 0.0529	0.0326 ± 0.0636	0.0485 ± 0.0734
Cohen's d	0.2232	0.3136	0.3331	0.2574	0.3344
Insufficiently grasped	0.043 ± 0.103	0 ± 0	0.0140 ± 0.0469	0 ± 0	0.0297 ± 0.0611
Target grasped	0.079 ± 0.112	0.0026 ± 0.0115	0.0248 ± 0.0529	0.0326 ± 0.0636	0.0485 ± 0.0734
Cohen's d	0.3313	0.3136	0.3331	0.6623	0.3570
Collision Max Depth (mm)					
No Haptics	4.69 ± 8.89	0.60 ± 0.76	2.92 ± 2.92	0.52 ± 0.52	1.78 ± 4.33
Haptics	4.59 ± 8.26	1.11 ± 1.11	1.87 ± 1.87	1.23 ± 1.23	2.85 ± 6.40
Cohen's d	-0.0113	0.3459	-0.0325	0.2229	0.1951
First	3.71 ± 6.44	1.15 ± 1.15	0.68 ± 0.68	1.23 ± 1.23	2.15 ± 5.83
Subsequent	5.57 ± 10.19	0 ± 0	4.11 ± 4.11	0.99 ± 0.99	2.47 ± 5.95
Cohen's d	0.1581	0.3359	-0.1718	0.4753	0.2850
Insufficiently grasped	3.73 ± 8.31	0 ± 0	1.29 ± 1.29	0 ± 0	0.38 ± 0.38
Target grasped	4.59 ± 8.22	0.76 ± 0.77	2.37 ± 2.92	1.31 ± 1.31	2.85 ± 5.77
Cohen's d	0.1581	0.3359	-0.1718	0.4753	0.2850
Average Depth (mm)					
No Haptics	2.10 ± 4.20	0.20 ± 1.10	1.10 ± 2.40	0.50 ± 1.30	1.60 ± 3.10
Haptics	2.30 ± 5.10	0.10 ± 0.80	1.40 ± 2.90	0.60 ± 1.70	1.80 ± 3.40
Cohen's d	-0.1000	0.2000	-0.0800	-0.0500	-0.0600
First	2.50 ± 4.60	0.30 ± 1.20	1.50 ± 3.20	0.60 ± 1.60	2.00 ± 3.70
Subsequent	1.80 ± 3.90	0.10 ± 0.90	1.00 ± 2.10	0.40 ± 1.00	1.20 ± 2.80
Cohen's d	-0.1400	0.1800	-0.0900	-0.1100	-0.1200
Insufficiently grasped	2.30 ± 4.30	0.20 ± 1.00	1.30 ± 2.60	0.60 ± 1.50	1.90 ± 3.20
Target grasped	2.00 ± 3.50	0.10 ± 0.70	1.10 ± 2.20	0.50 ± 1.10	1.50 ± 2.60
Cohen's d	-0.0700	0.1000	-0.0600	-0.0700	-0.0800

TABLE II: Not fully grasped, Find to Best, haptic influence comparison

Variable	No Haptics	Haptics	Cohen's d
Time(s)	22.71 ± 17.59	19.26 ± 9.84	-0.26
Vol. in Gripper (mm^3)	0.16 ± 0.20	0.42 ± 0.27	1.04
Alignment (Norm.)	0.35 ± 0.87	0.37 ± 0.67	0.02
Angle (Norm.)	-0.13 ± 0.26	0.05 ± 0.30	0.61
Collision freq. (Hz)	0.06 ± 0.13	0.21 ± 0.65	0.30
Max. Depth (mm)	5.05 ± 9.71	2.53 ± 7.47	-0.30
Average Depth (mm)	2.85 ± 1.68	1.35 ± 1.38	-1.03

Regarding the volume of the target inside the gripper, without haptic feedback, there is a 27% increase at the "Best" position, but the standard deviation is notably higher. As expected, there is a 69% difference between attempts that managed to insert the object and those that did not at the "Enter" moment.

In terms of errors, all Cohen's d values are below 0.2, indicating low significance in the difference of the values.

It can be observed that with haptic feedback, there was a slight increase in collisions. These are approximately 18 percent more frequent with haptic feedback, 2 percent less severe, and 8 percent deeper on average.

VII. Conclusion

This study contributed to the development of transmitting information through the sense of touch, addressing the challenge of limited dexterity in teleoperation tasks caused by the lack of sensory feedback and visual occlusion. By integrating haptic feedback through the adaptive triggers of a DualSense controller, we provided real-time tactile information to the operator based on the proximity of objects to the robot's end effector. Our system simulated the environment and the robot, virtually enlarged objects, and calculated overlapping volumes to adjust button stiffness proportionally.

The experimental results show cases with significant benefits of incorporating haptic feedback. When the target wasn't fully grabbed, operators using haptic feedback reached the "Best" position 28% faster compared to those without it. The percentage of the target inside the gripper was notably higher, indicating improved awareness of the object's relative position. Centering and alignment errors were closer to zero with haptic feedback, indicating that neither the robot nor the object get heavily damage in the interaction because of a proper grab position. Although the collision frequency remained similar, the severity of collisions, both maximum and average, were reduced when haptic feedback was employed.

These findings suggest that haptic feedback enhances the operator's situational awareness and ability to make informed decisions, leading to more intuitive and safer teleoperation. However, the performance metrics of our approach did not contribute to reduce collision risks. The approach considers real-world uncertainties and communication delays, and offers a low complexity alternative, avoiding meshes calculation or normal forces from surfaces.

Future work could focus on offering a more notorious notification for the user to avoid collision, or to recognize when it happens, like to convey in real-time vibration. Additionally, explore the system's effectiveness in more complex or real-world teleoperation scenarios. Overall, this approach significantly improves the user's awareness of the robot's interactions with its environment, making teleoperation tasks more efficient and safer.

References

[1] Application of Adaptive Controllers in Teleoperation Systems: A Survey. (2014). IEEE Transactions on Human-Machine Systems, 44(3), 337–352. doi:10.1109/thms.2014.2303983

[2] Jean Vertut and Philippe Coiffet. 1986. Teleoperations and robotics: evolution and development. Prentice-Hall, Inc., USA.

[3] R. R. Ma and A. M. Dollar.On dexterity and dexterous manipulation.In 15th International Conference on Advanced Robotics: New Boundaries for Robotics, ICAR 2011, Tallinn, Estonia, June 20-23, 2011., pages 1–7, 2011.

[4] Makofske, B., & Power, E. (2018). Manual Dexterity. Encyclopedia of Clinical Neuropsychology, 2080–2081. doi:10.1007/978-3-319-57111-9_1460

[5] Darvish, K., et al. (2023). Teleoperation of Humanoid Robots: A Survey.10.48550/arXiv:2301.04317.

[6] T. M. Lam, H. W. Boschloo, M. Mulder, and M. M. van Paassen, "Artificial Force Field for Haptic Feedback in UAV Teleoperation," *IEEE Transactions on Systems, Man, and Cybernetics - Part A: Systems and Humans*, vol. 39, no. 6, pp. 1316–1330, 2009, doi:10.1109/tsmca.2009.2028239.

[7] X. Hou, X. Wang, and R. Mahony, "Haptics-aided path planning and virtual fixture based dynamic kinesthetic boundary for bilateral teleoperation of VTOL aerial robots," in *Proceedings of the 2016 35th Chinese Control Conference (CCC)*, Chengdu, China, 2016, pp. 4705–4710, doi: 10.1109/ChiCC.2016.7554082.

[8] M. Coffey and A. Pierson, "Collaborative Teleoperation with Haptic Feedback for Collision-Free Navigation of Ground Robots," in *Proceedings of the 2022 IEEE/RSJ International Conference on Intelligent Robots and Systems (IROS)*, Kyoto, Japan, 2022, pp. 8141–8148, doi: 10.1109/IROS47612.2022.9981426.

[9] A. Gottardi, S. Tortora, E. Tosello, and E. Menegatti, "Shared control in robot teleoperation with improved potential fields," *IEEE Transactions on Human-Machine Systems*, vol. 52, no. 3, pp. 410–422, 2022.

[10] K. J. Kuchenbecker, W. R. Provancher, G. Niemeyer, and M. R. Cutkosky, "Haptic display of contact location," in *Proceedings of the 12th International Symposium on Haptic Interfaces for Virtual Environment and Teleoperator Systems*, 2004, doi:10.1109/haptic.2004.1287176.

[11] C. Ju and H. Son, "Evaluation of haptic feedback in teleoperated unmanned ground vehicle performance in obstacle avoidance scenario," *International Journal of Control, Automation and Systems*, vol. 17, no. 1, pp. 168–180, 2019, doi:10.1007/s12555-017-0721-y.

[12] T.-C. Lin, A. U. Krishnan, and Z. Li, "Comparison of haptic and augmented reality visual cues for assisting telemanipulation," in *Proceedings of the 2022 IEEE International Conference on Robotics and Automation (ICRA)*, Philadelphia, PA, USA, 2022, doi: 10.1109/ICRA46639.2022.9811669.

[13] Siciliano, Bruno & Sciavicco, L. & Luigi, Villani & Oriolo, G.. (2009). Robotics: Modelling, planning and control.

[14] M. Abramowitz and I. A. Stegun, Eds., Handbook of Mathematical Functions with Formulas, Graphs, and Mathematical Tables, 9th ed. New York: Dover, 1972, pp. 925-964.

[15] S. Strobl, A. Formella, and T. Pöschel, "Exact calculation of the overlap volume of spheres and mesh elements," Journal of Computational Physics, vol. 311, pp. 158-172, Feb. 2016, doi: 10.1016/j.jcp.2016.02.003.

[16] Intel Corporation, "Intel RealSense Depth Camera D435," [Online]. Available: https://www.intelrealsense.com/depth-camera-d435/

[17] S. Kojima, T. Nara, T. Takahashi, R. Bezerra, K. Gunji, K. Oguma, K. Hattori, R. Egawa, K. Ryotaro, and Y. Suzuki, "RoboCup Rescue 2023 Team Description Paper Quix," RoboCup Rescue 2023 TDP Collection 1, 2023. [Online]. Available: https://tdp.robocup.org/wp-content/uploads/tdp/robocup/2023/robocuprescue-robot/quix-479/robocup-2023-robocuprescue-robot-quixuMKVoch70B.pdf